Mon. Not. R. Astron. Soc. **355,** 1091–1104 (2004) doi:10.1111/j.1365-2966.2004.08383.x

Cosmological simulations of the intracluster medium

Scott T. Kay,[1⋆] Peter A. Thomas,[1] Adrian Jenkins[2] and Frazer R. Pearce[3]

[1]*Department of Physics and Astronomy, University of Sussex, Falmer, Brighton BN1 9QH*
[2]*Institute for Computational Cosmology, Physics Department, University of Durham, South Road, Durham DH1 3LE*
[3]*Physics and Astronomy Department, University of Nottingham, Nottingham NG7 2RD*

Accepted 2004 September 6. Received 2004 September 3; in original form 2004 July 2

ABSTRACT

We investigate the properties of the intracluster medium (ICM) that forms within N-body/hydrodynamical simulations of galaxy clusters in a ΛCDM cosmology. When radiative cooling and a simple model for galactic feedback are included, our clusters have X-ray luminosities and temperatures in good agreement with observed systems, demonstrating the required excess entropy in their cores. More generally, cooling and feedback increases the entropy of the ICM everywhere, albeit without significantly affecting the slope of the profile ($S \propto r$) at large radii. The temperature of the ICM is only modestly increased by these processes, with projected temperature profiles being in reasonable agreement with the observations. Star/galaxy formation is still too efficient in our simulations, however, and so our gas mass fractions are around 60 per cent of the observed value at r_{2500}. Finally, we examine the reliability of using the hydrostatic equilibrium equation to estimate cluster masses and find that it underpredicts the true mass of our clusters by up to 20 per cent, due to incomplete thermalization of the gas. Feedback reduces this discrepancy, however, with estimates being accurate to within 10 per cent out to r_{500}.

Key words: hydrodynamics – methods: numerical – X-rays: galaxies: clusters.

1 INTRODUCTION

Clusters of galaxies play an important role in our quest for determining the cosmology of our Universe. In models of hierarchical structure formation such as the ΛCDM model, the mass function of clusters is a sensitive function of cosmological parameters, notably the matter density parameter, $\Omega_{\rm m}$ and the amplitude of linear fluctuations on $8\,h^{-1}$ Mpc scales, σ_8. As a result, many authors have combined the observed (in the X-ray) abundance of clusters with theoretical mass functions (Press & Schechter 1974; Jenkins et al. 2001; Sheth, Mo & Tormen 2001) to constrain these parameters (e.g. Evrard 1989; Henry & Arnaud 1991; Oukbir & Blanchard 1992; White, Efstathiou & Frenk 1993a; Eke, Cole & Frenk 1996; Viana & Liddle 1996; Henry 2000; Pierpaoli et al. 2003; Viana et al. 2003).

In the post-*WMAP* era (Spergel et al. 2003; Verde 2003), particular attention is now being paid to systematic uncertainties that may bias these estimates. As was recently pointed out by Henry (2004), the largest systematic uncertainty in determining σ_8 using X-ray clusters is in the calibration of the X-ray temperature-to-mass relation. In order for robust determinations of such quantities to be made, accurate theoretical predictions for how clusters form and evolve are required, taking full account of the physics that govern the structure of the intracluster medium (ICM).

The best tool we have at our disposal to model the ICM is direct numerical simulation. Evrard (1990) performed the first cosmological simulation of a cluster and in his pioneering study demonstrated that many of its properties resembled those derived from X-ray observations. Subsequent studies that followed (e.g. Katz & White 1992; Thomas & Couchman 1992; Cen & Ostriker 1994; Navarro, Frenk & White 1995; Evrard, Metzler & Navarro 1996; Bryan & Norman 1998; Eke, Navarro & Frenk 1998; Frenk et al. 1999; Thomas et al. 2001) have significantly improved our understanding of X-ray clusters within hierarchical models.

Many of the first cluster simulations ignored radiative cooling of the gas on the grounds that clusters today have average cooling times longer than the age of the Universe. These 'non-radiative' simulations vindicated simple self-similar scaling relations, as expected when the structure of the ICM is determined solely by gravity (Kaiser 1986). As useful as non-radiative simulations have been, however, they contradict X-ray observations of clusters. The clearest example is the luminosity–temperature ($L_{\rm X}$–$T_{\rm X}$) relation that is observed to have a steeper slope ($L_{\rm X} \propto T_{\rm X}^{\sim 3}$, e.g. Edge & Stewart 1991) than predicted from gravitational heating models ($L_{\rm X} \propto T_{\rm X}^2$). Another useful viewpoint is that the ICM is less concentrated because its entropy is higher (Evrard & Henry 1991; Kaiser 1991), as demonstrated by Ponman, Cannon & Navarro (1999). Consequently, much attention has been paid to models which focus on

⋆E-mail: s.t.kay@sussex.ac.uk

the entropy of the ICM (see, e.g. Bower 1997; Voit & Bryan 2001; Voit et al. 2002, 2003a).

Early models concentrated on the *pre-heating* hypothesis, that the ICM was heated externally when the density contrast was low, therefore requiring less energy to reach the desired entropy level than if the heating occurred in a denser environment. Simulations of pre-heating models have been shown to be capable of producing the desired effect on the overall entropy level of the ICM (e.g. Navarro et al. 1995; Bialek, Evrard & Mohr 2001; Borgani et al. 2002) but have since fallen out of favour for many reasons; for example, they predict isentropic cores in low-mass clusters that are not observed (see Ponman, Sanderson & Finoguenov 2003).

More recently, attention has shifted to modelling the effects of radiative cooling on the ICM. Naively, since the entropy of cooling gas decreases, one would expect cooling to have the opposite of the desired effect on the ICM, making clusters even more luminous than when cooling is neglected. Indeed, this effect was seen in some numerical studies (Katz & White 1992; Suginohara & Ostriker 1998; Lewis et al. 2000), but was caused by the presence of an unrealistically large central galaxy. Pearce et al. (2000) demonstrated that this 'overcooling' problem could be ameliorated by 'decoupling' the hot gas from the cold galactic gas, and as a result, found that cooling actually increased the ICM entropy. Most of the galactic material cools very quickly at high redshift without ever reaching the virial temperature (Binney 1977; Kay et al. 2000; Binney 2004), and instead emits in the ultraviolet (Fardal et al. 2001). The ICM adjusts itself to the loss of pressure support, with higher-entropy gas flowing inwards to replace the cooled gas (Pearce et al. 2000). Various subsequent studies of cooling have successfully reproduced various observed X-ray properties of clusters (e.g. Bryan 2000; Muanwong et al. 2001, 2002; Davé, Katz & Weinberg 2002; Thomas et al. 2002; Voit et al. 2002; Wu & Xue 2002).

Although cooling contributes to the excess entropy of the ICM, heating processes (from stars and/or active galactic nuclei) are still required in order to regulate galaxy formation and possibly shape their luminosity function (e.g. Cole 1991; White & Frenk 1991; Balogh et al. 2001; Benson et al. 2003; Binney 2004). Numerical efforts are now focusing on incorporating such feedback processes with cooling into simulations of groups and clusters (Kay, Thomas & Theuns 2003; Tornatore et al. 2003; Borgani et al. 2004; Kay 2004) and will continue to remain a vital area of study for the foreseeable future, until the effects of galaxy formation can be successfully incorporated into ICM models.

In this paper we focus on a set of high-resolution cosmological simulations of 15 galaxy clusters, with the primary aim of investigating how the combined effects of radiative cooling and a simple model for targeted heating by galactic feedback affects the structure of the ICM, and as a consequence, estimates of the total mass distribution in clusters. Our study is in many ways similar to, and can be viewed as a progression of, those performed by Ascasibar et al. (2003) and Rasia, Tormen & Moscardini (2004), who restricted their simulations to non-radiative systems. We compare our findings with their results and with observational data where appropriate.

The rest of this paper is organized as follows. In Section 2 we outline our method and discuss general properties of our simulated clusters. Radial profiles derived from the distribution of cluster mass (total mass density, ICM density, entropy and gas fraction) are discussed in Section 3. In Section 4 we present cluster temperature profiles. Cluster mass determinations are investigated under various conditions in Section 5. Finally, we draw conclusions in Section 6.

2 SIMULATION DETAILS

Simulations were performed assuming a ΛCDM cosmology, setting $\Omega_{\rm m} = 0.3$, $\Omega_\Lambda = 0.7$, $\Omega_{\rm b} = 0.045$, $h = 0.7$ and $\sigma_8 = 0.9$. Our choice of parameters is in reasonably good agreement with the *WMAP* results (Spergel et al. 2003).

All simulations were performed with version 2 of the GADGET *N*-body/hydrodynamics code (Springel, Yoshida & White 2001), kindly made available to us by V. Springel. Gravitational forces were computed using the combination of particle-mesh and tree algorithms. Hydrodynamical forces were calculated using the variant of the smoothed particle hydrodynamics (SPH) algorithm proposed by Springel & Hernquist (2002) that explicitly conserves entropy where the (artificial) viscosity of the flow is zero.

Two sets of simulations were used in this study. First of all, we performed simulations of a random volume, sampling a cube of comoving length, $L = 120\,h^{-1}$ Mpc using $N = 2 \times 256^3$ particles (half baryons, half dark matter). The dark matter and baryon particle masses are then $m_{\rm dark} = 7.3 \times 10^9\,h^{-1}\,{\rm M}_\odot$ and $m_{\rm bary} = 1.3 \times 10^9\,h^{-1}\,{\rm M}_\odot$, respectively. The second set of simulations consisted of 10 resimulated clusters, selected from a large *N*-body simulation performed by the Virgo Consortium (Yoshida, Sheth & Diaferio 2001), with $N = 512^3$ and $L = 479\,h^{-1}$ Mpc. The 10 most massive objects with virial masses below $10^{15}\,h^{-1}\,{\rm M}_\odot$ were selected and resimulated at higher resolution, with similar particle masses to the random volume simulations. This sample has already been studied elsewhere without gas (see, e.g. Gao et al. 2004).

For all simulations, we started the runs at $z = 49$ and evolved them to $z = 0$ (our results are presented for this redshift). We fixed the gravitational softening in comoving coordinates at all times to an equivalent Plummer value of $\epsilon = 20\,h^{-1}$ kpc (GADGET uses a spline softening kernel where the force becomes exactly Newtonian for $r > 2.8\epsilon$).

2.1 The models

In this paper we focus on two models, differing only in the freedom allowed for the entropy[1] of the gas to vary. In the first model, hereafter referred to as the *non-radiative* model, entropy can only increase due to shock heating. Although it has already been demonstrated that this model does not produce clusters that resemble observed systems (e.g. Evrard & Henry 1991) it nevertheless has been a well-studied model and provides a good reference to measure the effects of non-gravitational processes on the ICM.

In the second model, hereafter the *feedback* model, we included two additional physical processes, both thought to be crucial in producing realistic clusters. First of all, the gas was allowed to lose entropy through radiative cooling. Although clusters at low redshift have average cooling times that are longer than the age of the Universe, the same cannot be said for their precursors at high redshift when most of their galaxies form. The result of this removal of low-entropy gas is a net increase in the entropy of the remaining ICM (Pearce et al. 2000). We included radiative cooling using the same method as used in the HYDRA code (see Thomas & Couchman 1992), adopting a tabulated cooling function (Sutherland & Dopita 1993) with $Z = 0.3\,{\rm Z}_\odot$.

[1] We define entropy as $S = kT(\rho/\mu m_{\rm H})^{1-\gamma}$, where $\gamma = 5/3$ is the ratio of specific heats for a monatomic ideal gas and $\mu\,m_{\rm H} = 0.6$ is the mean atomic weight of a fully ionized plasma.

Gas is able to cool down to 10^4 K, where we arbitrarily cut off the cooling rate. The physics that govern the fate of this cooled gas, now identified as galactic material (e.g. Kay et al. 2000), is complex and would not be resolved in our simulations (although see, e.g. Springel & Hernquist 2003 for an attempt to model a multiphase galactic component within cosmological simulations). We instead adopt a phenomenological approach to galaxy formation, and assume that a fixed mass fraction of cooled gas will go on to form stars and the rest will be reheated by the stars (the heating could also be due to active galactic nuclei, but note our model does not allow us to discriminate between the two).

First, we identify cooled gas using a density threshold, $n_{\rm H} > n_*$ (where $n_{\rm H} = X\rho/m_{\rm H}$ is the hydrogen density and $X = 0.76$ the hydrogen mass fraction), and a temperature threshold, $T < T_*$, setting $n_* = 10^{-3}\,{\rm cm}^{-3}$ and $T_* = 1.2 \times 10^4$ K. Although typical densities where star/black hole formation occurs are much higher, we deliberately set the threshold to be low as it ensures that a negligible amount of thermal energy in the reheated gas is lost as radiation. Note therefore that we will be ignoring some cold gas that would otherwise be ablated by the ICM.

Whether a particle then forms stars or is reheated is determined on a stochastic basis. The mass fraction of reheated gas is controlled by a parameter $f_{\rm heat}$ (hence a fraction, $1 - f_{\rm heat}$, will form stars). For each cooled gas particle we draw a random number, r, from the unit interval and increase its entropy by a fixed amount, $S_{\rm heat}$, if $r < f_{\rm heat}$. The temperature of the reheated gas is then

$$kT_{\rm heat} = \left(\frac{S_{\rm heat}}{100\,{\rm keV\,cm^2}}\right)\left(\frac{n_{\rm heat}}{10^{-3}\,{\rm cm^{-3}}}\right)^{2/3}\ {\rm keV}. \quad (1)$$

We adopted a choice of parameters equivalent to that used by Kay (2004) in his *strong feedback* model, namely $S_{\rm heat} = 1000\,{\rm keV\,cm^2}$ and $f_{\rm heat} = 0.1$. For gas with density, $n_{\rm H} = n_*$, $kT_{\rm heat} = 17$ keV, although part of this energy is distributed as the gas does work on its neighbours.

This energy is only carried by 10 per cent of the mass of cooled gas, so it is useful to estimate the overall energy deposited into the ICM. Such an estimate is

$$E_{\rm ICM} = \frac{3}{2}\frac{kT_{\rm heat}}{\mu m_{\rm H}} M_{\rm heat}, \quad (2)$$

where $M_{\rm heat} = (f_{\rm heat}^{-1} - 1)^{-1} M_*$ is the mass of reheated gas, directly related to the residual mass of stars in the cluster, M_*. For our choice of parameters, $E_{\rm ICM} \sim 10^{63}(M_*/10^{14}\,{\rm M}_\odot)$ erg, comparable with the maximum energy available from Type II supernovae, assuming one supernova releases 10^{51} erg and the number of Type II supernovae is $N_{\rm SNII} = 0.01(M_*/\,{\rm M}_\odot)$. Thus, on average, the energy added to each ICM atomic nucleus is $kT_{\rm ICM} = 3.1(f_*/f_{\rm gas})$ keV, where f_* and $f_{\rm gas}$ are the star and ICM mass fractions, respectively. For clusters in our *feedback* model, we find $kT_{\rm ICM} \sim 1$ keV, i.e. a similar level to that found in previous studies including heating (e.g. Wu, Fabian & Nulsen 2000; Borgani et al. 2001; Bower et al. 2001; Muanwong et al. 2002).

2.2 Cluster identification

Clusters were identified using the procedure detailed in Muanwong et al. (2002). This involved finding the cluster centre (by searching for the density maximum) then growing spheres around this centre until the average density reached a constant factor, Δ, times the critical density. This threshold defines the relation between cluster mass and radius

$$M_\Delta = \frac{4\pi}{3}\,\Delta\,\rho_{\rm cr}\,R_\Delta^3, \quad (3)$$

where $\rho_{\rm cr} = 3H_0^2/8\pi\ G$ is the critical density and $H_0 = 70\,{\rm km s^{-1}\,Mpc^{-1}}$ for our cosmology. We define the virial mass/radius using $\Delta = 178\,\Omega_{\rm m}^{0.45} \sim 104$ (Eke et al. 1998). Our main results will refer to virial quantities but occasionally we will use other values of Δ where appropriate.

We only considered clusters with $M_{\rm vir} > 4.3 \times 10^{14}\,h^{-1}\,{\rm M}_\odot$, corresponding to an effective particle number threshold, $N = M_{\rm vir}/(m_{\rm dark} + m_{\rm gas}) > 50\,000$, as suggested by Borgani et al. (2002) for obtaining reliable X-ray properties. All our resimulated clusters and the five most massive objects in our random volume simulations satisfied this criterion, bringing our sample to 15 clusters per model.

2.3 Cluster sample and global properties

Table 1 lists global properties of our 15 *feedback* clusters. The systems span a factor of 4 in mass, with $kT_{\rm vir} \sim 4$–8 keV. We define the ICM as all gas particles within $R_{\rm vir}$ with $kT > 0.1$ keV (i.e. $\sim 1.2 \times 10^6$ K). Generally, very little or no gas exists in our clusters below this temperature threshold (in the *feedback* model, a few gas particles exist that have cooled down to $T = 10^4$ K but have not yet formed stars or been reheated).

There is very little scatter between ICM gas fraction values, $f_{\rm gas} = 0.100 \pm 0.005$ (for the *non-radiative* clusters, $f_{\rm gas} = 0.136 \pm 0.004$). We note the average star fraction, $f_* = 0.035 \pm 0.002$, i.e. $\sim$25 per cent of the baryon mass is collisionless. By construction, this fraction is lower than would be expected in the absence of feedback; however, it is still higher than the observed stellar mass fraction, measured to be $\lesssim$15 per cent (e.g. Balogh et al. 2001; Lin, Mohr & Stanford 2003). The observed value is an underestimate of f_*, as part of this mass may be hidden in a diffuse component (e.g. Murante et al. 2004); however, note that the desired amount of cooled baryons can be achieved in our model by increasing $f_{\rm heat}$, without significantly affecting the global properties of the ICM (Kay et al. 2003).

To illustrate the difference between the X-ray properties of the clusters in the two models, we show in Fig. 1 the $L_{\rm X}$–$T_{\rm X}$ relation at $z = 0$. *Non-radiative* clusters are represented by open squares

Table 1. Global parameters of the simulated cluster sample, from left to right: cluster number; virial radius, in h^{-1} Mpc; virial mass in $10^{14}\,h^{-1}\,{\rm M}_\odot$; virial temperature in keV; number of baryon particles (gas or stars) within $R_{\rm vir}$; ICM gas mass fraction; stellar mass fraction.

No.	$R_{\rm vir}$	$M_{\rm vir}$	$kT_{\rm vir}$	$N_{\rm bary}$	$f_{\rm gas}$	f_*
1	2.41	16.83	7.70	184 082	0.105	0.035
2	2.03	10.08	4.91	92 833	0.102	0.032
3	2.02	9.82	6.06	88 840	0.097	0.035
4	1.99	9.44	5.57	86 347	0.098	0.035
5	1.99	9.43	6.00	89 872	0.105	0.034
6	1.96	9.03	5.10	84 546	0.103	0.033
7	1.94	8.68	6.57	82 922	0.104	0.035
8	1.82	7.24	4.34	75 390	0.098	0.036
9	1.80	6.93	4.73	68 042	0.108	0.035
10	1.79	6.91	4.66	62 766	0.097	0.035
11	1.78	6.80	4.97	64 532	0.104	0.034
12	1.73	6.22	4.02	56 027	0.096	0.035
13	1.70	5.88	3.74	62 316	0.100	0.036
14	1.67	5.56	4.54	56 040	0.091	0.038
15	1.59	4.77	3.99	48 156	0.091	0.038

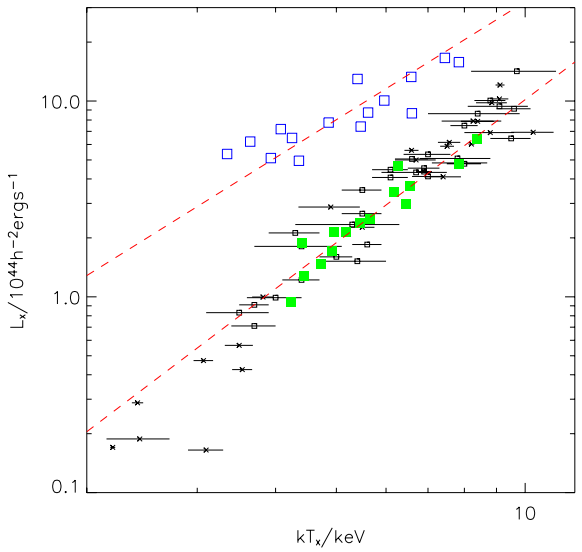

Figure 1. X-ray luminosity–temperature relation for clusters in the *non-radiative* (open squares) and *feedback* (filled squares) models. Dashed lines are power-law fits to the data (assuming $L_X \propto T_X^2$ for the *non-radiative* clusters). Symbols with error bars are for clusters studied by Markevitch (1998b) and Arnaud & Evrard (1999).

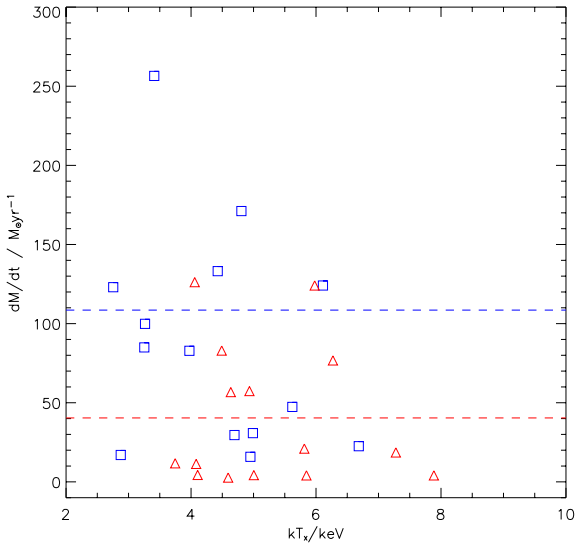

Figure 2. Mass deposition rates for the *non-radiative* (squares) and *feedback* (triangles) clusters, inferred from their core X-ray emission, as a function of emission-weighted temperature. Dashed lines give the mean rates.

and *feedback* clusters by filled squares. X-ray emission-weighted temperatures and luminosities were computed using the procedure outlined by Muanwong et al. (2002). To be approximately consistent with the observational data, luminosities are bolometric and temperatures calculated in a hard (1.5–8.0 keV) X-ray band. Furthermore, emission from within $50\,h^{-1}$ kpc of the cluster centre was omitted (i.e. we removed excess emission present due to cooling flows).

The upper dashed line illustrates a best-fitting power law to the *non-radiative* clusters, assuming $L_X \propto T_X^2$. This is the expected scaling relation for self-similar clusters assuming the dominant emission mechanism is thermal bremsstrahlung (Kaiser 1986); our clusters are in reasonable agreement with this scaling.

Cooling and feedback processes combine to reduce the emission from within each cluster, particularly in low-temperature systems (see Kay 2004). This lowers and steepens the L_X–T_X relation, bringing the *feedback* clusters into good agreement with the observational data (Arnaud & Evrard 1999; Markevitch 1998b). The best-fitting relation for these systems is $\log(L_{X,44}) = (-1.42 \pm 0.17) + (2.43 \pm 0.23)\,\log(kT_X/\mathrm{keV})$, where $L_{X,44}$ is L_X in units of $10^{44}\ h^{-2}\,\mathrm{erg\,s^{-1}}$.

Recently, it has emerged from X-ray spectra that there is a lack of cool gas (below one-third of the mean temperature) in the cores of clusters, even though the temperature of the gas is decreasing radially inwards and its cooling time is significantly shorter than a Hubble time (e.g. Fabian 2003). Such spectroscopic mass-deposition rates, $\dot{M}_{\rm spec}$, are of order $10\,\mathrm{M_\odot\,yr^{-1}}$, about a factor of 5–10 lower than rates estimated directly from the core X-ray emission of a cluster

$$\dot{M}_X = \frac{2}{5}\,\frac{L_X\,\mu m_H}{kT_X}. \qquad (4)$$

Unfortunately our model clusters do not have the resolution for us to study their cooling flows in detail (a $10\,\mathrm{M_\odot\,yr^{-1}}$ cooling flow corresponds to one gas particle cooling approximately every 200 Myr), in particular, to measure $\dot{M}_{\rm spec}$. However, we can estimate the apparent mass deposition rate, $\dot{M}_X$. Fig. 2 illustrates such rates for our *non-radiative* and *feedback* clusters (calculated within $50\,h^{-1}$ kpc of the cluster centre). Note that both models exhibit a large spread in values: in the former case, $\dot{M}_X$ lies in the range 20–400 $\mathrm{M_\odot\,yr^{-1}}$ (although the gas can never cool), while in the latter case, $\dot{M}_X$ = 3–130 $\mathrm{M_\odot\,yr^{-1}}$. The *feedback* model, with $\langle\dot{M}_X\rangle = 40\,\mathrm{M_\odot\,yr^{-1}}$, is in broad agreement with the observations.

3 CLUSTER MASS PROFILES

Measuring the mass (both baryonic and total) distribution in clusters is of primary interest as it allows constraints to be placed on cosmological parameters, for example by calibrating the relation between mass and X-ray temperature (e.g. Henry 2004) or luminosity (e.g. Allen et al. 2003), or by using the gas mass fraction itself (e.g. White et al. 1993b; Evrard 1997; Allen, Schmidt & Fabian 2002; Allen et al. 2004). Knowledge of the ICM temperature distribution allows gas mass density profiles to be estimated via deconvolution of X-ray surface brightness profiles, and total masses estimated via the equation of hydrostatic equilibrium. We will return to the latter issue in Section 5, but for now we examine the mass distribution of our simulated clusters directly.

3.1 Mass density profiles

Shown in Fig. 3 are total mass density profiles, plotted as $x^2\rho(x)/\rho_{\rm cr}$, where $\rho_{\rm cr}$ is the critical density and $x = r/r_{\rm vir}$. We set the minimum radius to be $x_{\rm min} = 0.04$ as this radius is both larger than the spline gravitational softening length and contains at least 100 hot gas particles for all clusters in our sample (Borgani et al. 2002; Ascasibar et al. 2003). Solid curves represent the mean profile and the error on the mean while error bars illustrate standard deviations within each bin, highlighting cluster-to-cluster variations. The scatter in density about the mean at each radius is quite small for both models, $\sim \pm$ 15 per cent when averaged over all bins.

A useful one-parameter model was proposed by Navarro et al. (1995, 1997, hereafter NFW)

$$\frac{\rho(x)}{\rho_{\rm cr}} = \frac{\delta_c}{cx(1+cx)^2}, \qquad (5)$$

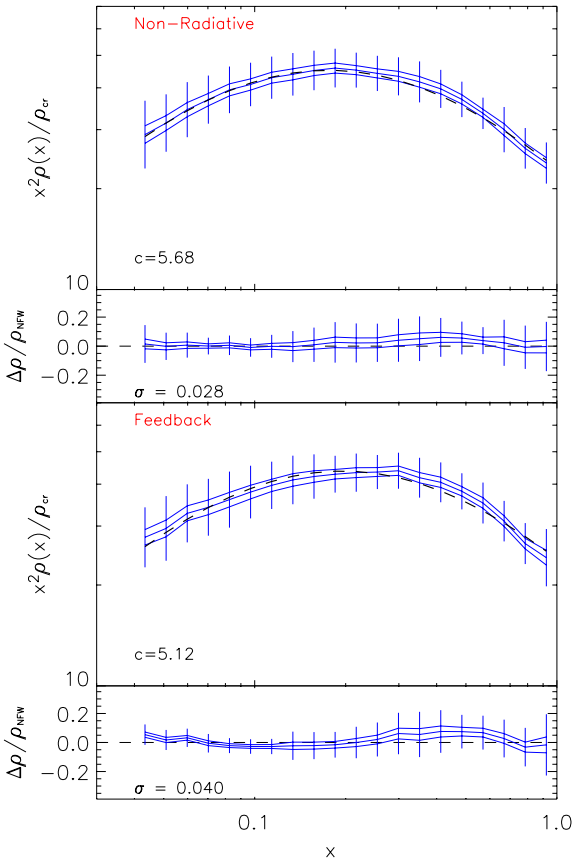

Figure 3. Total mass density profiles, $x^2\rho(x)$, where $x = r/r_{\rm vir}$, for clusters in the *non-radiative* and *feedback* models. Solid curves are the mean profile and the error on the mean, and the error bars illustrate the standard deviation within each bin. The dashed curve is the best-fitting NFW profile to the mean curve, weighted by the error on the mean, with the concentration parameter given in the legend. Also plotted below each main panel is the fractional differences between individual profiles and corresponding best-fitting NFW profiles. Again, the solid curve is the mean and the error bars the standard deviations within each bin. The rms fractional difference, averaged over all bins, is given in the legend.

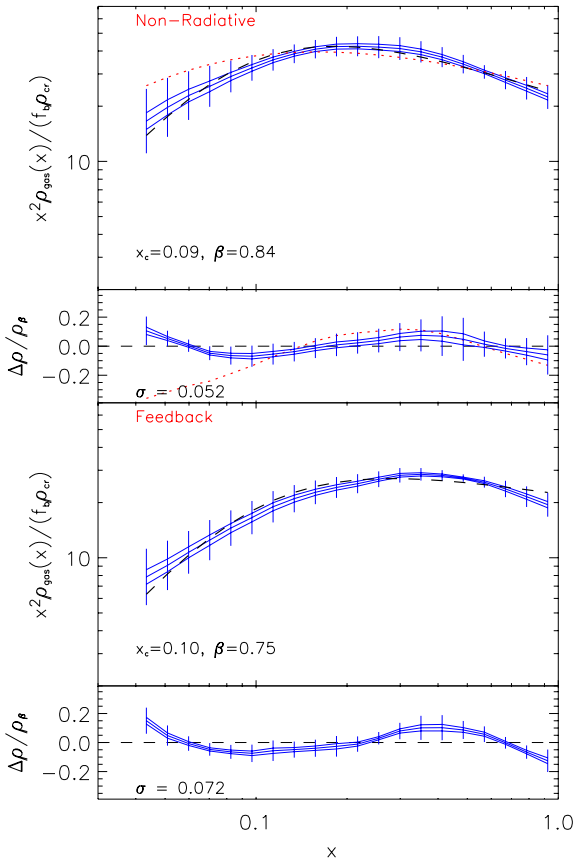

Figure 4. ICM density profiles, $x^2\rho_{\rm gas}(x)$, fitted using the isothermal β-model. The model profile fitted to the results of Rasia et al. (2004) is shown as a dotted curve.

where c is the concentration parameter and

$$\delta_{\rm c} = \frac{\Delta}{3}\,\frac{c^3}{\ln(1+c) - c/(1+c)}, \tag{6}$$

where $\Delta = 104$ in our case. Best-fitting NFW profiles to the mean density profiles, weighted by the error on the mean, are plotted as dashed curves in the figure. The mean profile concentration is 5.7 for the *non-radiative* model and 5.1 for the *feedback* model. Cooling and feedback slightly flatten the inner profile ($x < 0.3$), causing a $\sim$10 per cent increase in the best-fitting value of c.

In the lower panels of Fig. 3, we plot the fractional difference, $\Delta\rho/\rho$, between individual profiles and their corresponding NFW model fits. Again, the solid curve is the result for the mean profile and the error bars the standard deviation within each bin. Thomas et al. (2001) pointed out that, for their non-radiative clusters simulated in a τCDM cosmology, the NFW model generally does not provide a good fit to individual systems but does well when fitting a profile averaged over clusters with similar mass. For our clusters, the fit also improves significantly when averaging over clusters. The mean deviation at a given radius is around 10 per cent, but the root-mean-square difference, $\sqrt{\langle(\Delta\rho/\rho)^2\rangle}$, when averaged over all clusters and bins, is only a few per cent.

3.2 ICM density profiles

Fig. 4 illustrates ICM density profiles: comparing the two simulation models reveals that the *feedback* clusters have a lower density than the *non-radiative* clusters everywhere, with the difference being particularly pronounced in the central region. This is caused both by cooling (which removes gas from the ICM) and feedback (which heats the ICM). Since the cooling rate scales as ρ and the feedback rate effectively scales with the cooling rate, we expect their influence to be more pronounced closer to the cluster centre.

Historically, the isothermal β-model (Cavaliere & Fusco–Femiano 1976) is used to fit X-ray surface brightness profiles (we will return to this in Section 5), with the underlying ICM density profile being

$$\frac{\rho_{\rm gas}(x)}{f_{\rm b}\rho_{\rm cr}} = \frac{\delta_\beta}{(x^2 + x_{\rm c}^2)^{3\beta/2}}, \tag{7}$$

where $f_{\rm b} = \Omega_{\rm b}/\Omega_{\rm m}$, $x_{\rm c} = r_{\rm c}/r_{\rm vir}$ is the core radius and β determines the asymptotic slope at large radii. We confirm in Fig. 4, for both our simulation models, the finding by other authors (e.g. Ascasibar et al. 2003, hereafter AYMG; Rasia et al. 2004, hereafter RTM) that the model is not a good fit to the data, systematically overpredicting the slope of the profile at small radii and underpredicting it at large radii.

RTM suggested an alternative expression for the density profile, which we write as

$$\frac{\rho_{\rm gas}(x)}{f_{\rm b}\rho_{\rm cr}} = \frac{\delta_\alpha}{(x+x_{\rm p})^\alpha}, \quad (8)$$

where they fixed $x_{\rm p} = 0.04$ and $\alpha = 2.5$ (shown in Fig. 4 as a dotted curve). As can be seen, however, this profile does not provide a good fit to our data. A good fit can be achieved for our *non-radiative* clusters if we instead allow the data to select values for $x_{\rm p}$ and α; our results favour a steeper asymptotic slope ($\alpha \sim 3$) and the ICM in our clusters is less centrally concentrated than found by RTM. For the *feedback* clusters, equation (8) also improves the fit over the β-model, but still does not provide a satisfactory description of the data, again getting the slope wrong at large and small radii. We therefore caution the use of such expressions as a general tool in the modelling of clusters: a larger sample of clusters spanning a wider range in mass will be required in order to investigate this issue further.

3.3 ICM entropy profiles

The ICM entropy profile is a particularly useful quantity as it reveals information about the nature of non-gravitational processes in clusters (e.g. Evrard & Henry 1991; Kaiser 1991; Bower 1997; Voit & Bryan 2001; Voit et al. 2002, 2003a; Ponman et al. 2003; Voit & Ponman 2003b; Borgani et al. 2004; Kay 2004). Gravitational heating models, in which the outer entropy profile is determined by a spherical accretion shock, predicts an outer slope of 1.1 (Tozzi & Norman 2001). Observed entropy profiles exhibit similar values (e.g. Arnaud, Pratt & Pointecouteau 2004), suggesting that the main effect of non-gravitational processes is to increase the normalization of the entropy profile without significantly affecting its shape (see Ponman et al. 2003).

In Fig. 5 we present ICM entropy profiles, scaled by $S_{\rm vir} = kT_{\rm vir}(\mu m_{\rm H})^{2/3}(\Delta\rho_{\rm cr}\Omega_{\rm b}/\Omega_{\rm m})^{-2/3}$. The profiles are very close to power laws for $x > 0.2$. Our *non-radiative* clusters predict an outer slope of 1.2, very similar to that predicted by Tozzi & Norman's models, and consistent with a study of smaller systems, shown to be in good agreement with results from independent simulations using ENZO, an adaptive-mesh refinement code (Voit, Kay & Bryan 2004). Cooling and feedback increase the entropy distribution of the gas at all radii, acting to flatten the profiles: at $x = 1$ the increase is only 25 per cent but rises to almost a factor of 2 at $x = 0.2$. Note, however, the outer slope does not change significantly, $S \propto x$, and so is still similar to observational determinations.

3.4 Gas fraction profiles

A unique feature of cluster-sized haloes is that, in principle, most (if not all) of their baryonic content can be observed directly. Combined with an estimate of the total cluster mass, it is then possible to place constraints (in particular, an upper limit) on $\Omega_{\rm m}$, assuming a baryon density inferred from elsewhere, such as the nucleosynthetic value (White et al. 1993b).

Panels on the left of Fig. 6 illustrate cumulative ICM gas fraction profiles, $f_{\rm gas}(<x) = M_{\rm gas}(<x)/M_{\rm tot}(<x)$. As was found by previous authors (e.g. Eke et al. 1998; Frenk et al. 1999) the *non-radiative* profile appears to converge to a value close to, but not exactly, the global value at the virial radius (we find $f_{\rm gas} \sim 0.9\ \Omega_{\rm b}/\Omega_{\rm m}$). (The baryon fraction does not reach the global value until $x \sim 2$.) The rise is gradual: $f_{\rm gas}(x = 0.1) \sim 0.8\ f_{\rm gas}(x = 1)$.

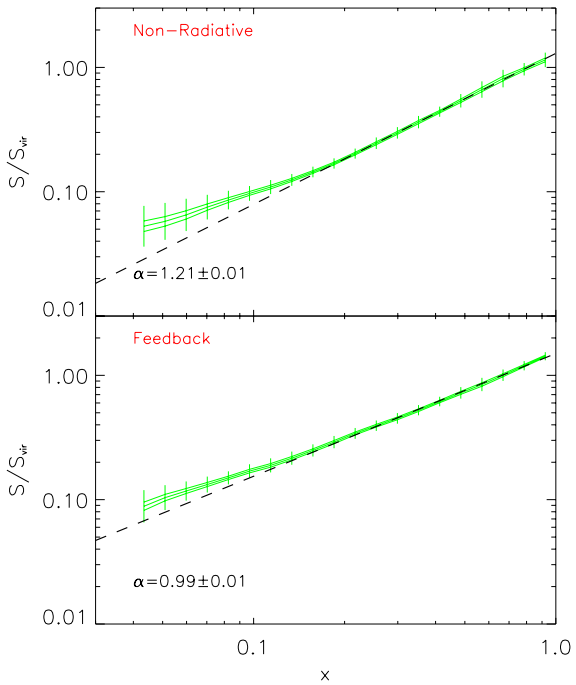

Figure 5. Dimensionless entropy profiles for clusters in the *non-radiative* (top) and *feedback* (bottom) models. The dashed line is the best-fitting power law to the mean profile for $0.2 < x < 1$ (the power-law index is given in the legend).

Gas fractions in the *feedback* clusters are ∼25 per cent lower at $x = 1$ due to radiative cooling: as can be seen from the right half of the figure, the total baryon fraction profiles reach the same value as in the *non-radiative* clusters. The increase in gas fraction with radius is also larger, $f_{\rm gas}(x = 0.1) \sim 0.6 f_{\rm gas}(x = 1)$, as a result of the gas being more extended due to its higher entropy.

Recently, Allen et al. (2004) measured gas fraction profiles for 26 relaxed X-ray luminous clusters observed with *Chandra*, out to $\Delta = 2500$. They found that the profiles rise from $f_{\rm gas} \sim 0.07$ at $x = 0$ to $f_{\rm gas} \sim 0.12$ at $x = 0.25$ (r_{2500}). These results are also shown in Fig. 6, plotted as squares. Intriguingly, the observational data resemble our *non-radiative* clusters more than our *feedback* clusters, with the latter having gas fractions that are around 60 per cent of the observed value at r_{2500}. We also show the error-weighted mean gas fraction at r_{200} ($x \sim 0.75$), as measured by Ettori (2003), consistent with the result of Allen et al. if the profiles do not continue to rise much beyond r_{2500}. Here, our *feedback* results are approximately 80 per cent of the observed estimate.

In the right-hand panels of Fig. 6 we plot *bias* factor profiles, $b = f_{\rm bary}/(\Omega_{\rm b}/\Omega_{\rm m})$, i.e. the baryon fraction, $f_{\rm bary}$, in units of the global value. Allen et al. assume a constant fraction (16 per cent) of baryons in stars. Interestingly, the *feedback* clusters are now in good agreement with their observations. Cooling leads to a rise in the central baryon fraction, flattening the profile with respective to the *non-radiative* case. Clearly, however, our *feedback* clusters have too much material in stars at all radii (f_* decreases monotonically with radius, from 0.54 at $x = 0.05$ to 0.25 at $x = 1$). At least part of the problem may be due to forming stars at artificially low densities: while increasing the star formation density threshold presents other problems (in particular, the propagation of feedback energy to lower-density regions), it will allow more gas to be ablated as it moves through the ICM, therefore reducing the amount of material available to form stars.

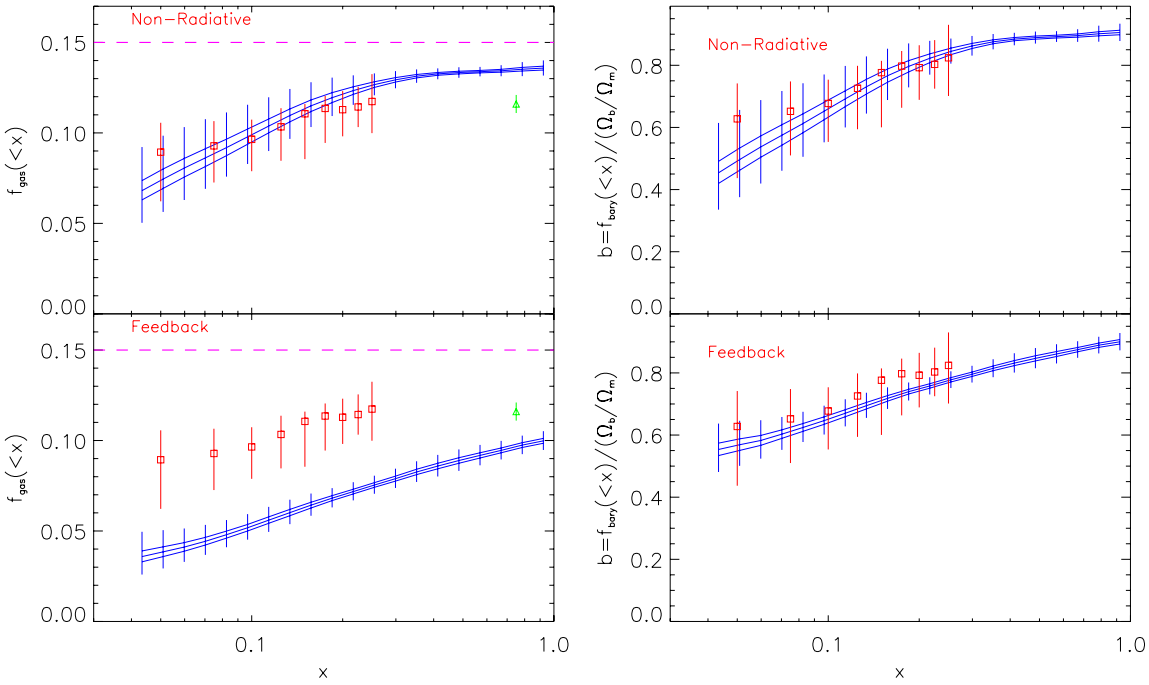

Figure 6. ICM gas fraction (left) and baryon fraction (right) profiles for clusters in the *non-radiative* and *feedback* models. The global baryon fraction, $\Omega_b/\Omega_m = 0.15$, is plotted as a horizontal dashed line. The triangle is the error-weighted mean measurement at r_{200} ($x \sim 0.75$) by Ettori (2003). Square symbols are data points from Allen et al. (2004).

4 TEMPERATURE PROFILES

A more accurate description of the ICM requires the spatial distribution of its temperature to be measured, which can be achieved using X-ray spectroscopy. Both observations and simulations concur that the ICM is non-isothermal, and so measuring temperature gradients improves the accuracy of estimating the mass of a cluster if it is in hydrostatic equilibrium.

Early observations of azimuthally averaged temperature profiles debated whether the inner profile was declining with radius (Markevitch et al. 1998a) or was isothermal (Irwin, Bregman & Evrard 1999; Irwin & Bregman 2000; White 2000). A later study by De Grandi & Molendi (2002) was consistent with isothermality outside cooling-flow regions and within $\sim 0.2\, r_{\rm vir}$. This was confirmed by Allen, Schmidt & Fabian (2001) for their sample of six luminous relaxed clusters observed with *Chandra*, and more recently by Arnaud et al. (2004) for seven clusters observed with *XMM–Newton*. Although the situation is still not robust, the general consensus is that the ICM temperature rises from the centre to $\sim 0.1 r_{\rm vir}$ is approximately isothermal then starts to decline beyond ~ 0.2–$0.3 r_{\rm vir}$. More high-quality data from *XMM–Newton* and *Chandra* will improve the situation considerably.

4.1 3D temperature profiles

We first present 3D temperature profiles, shown in Fig. 7. Each profile is scaled by the isothermal model virial temperature of the cluster, $T_{\rm vir} = G\mu m_{\rm H} M_{\rm vir}/2\, kR_{\rm vir}$. For the *non-radiative* clusters, our results are in good agreement with previous numerical studies (e.g. Evrard 1990; Navarro et al. 1995; Eke et al. 1998), i.e. the profile slowly varies out to $x \sim 0.2$, then declines by around a factor of 2 out to $x = 1$. A more contentious issue is whether the inner profile is isothermal (e.g. RTM) or continues to rise to the centre (e.g. AYMG). We find our average *non-radiative* profile is isothermal within

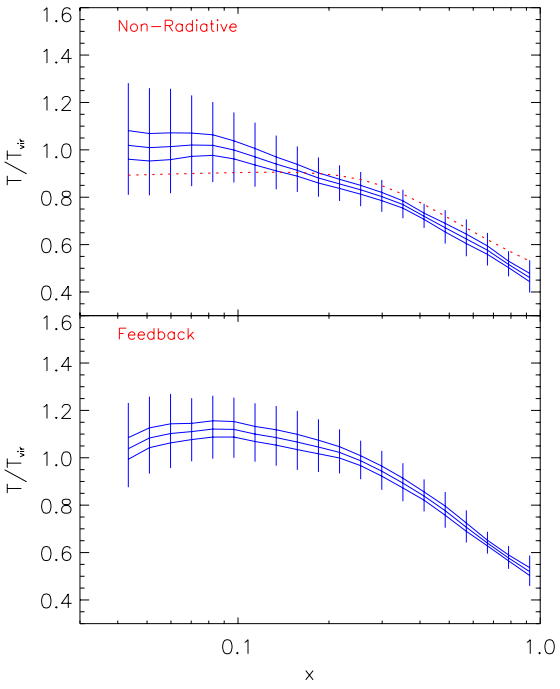

Figure 7. Dimensionless temperature profiles for clusters in the *non-radiative* and *feedback* models. The best-fitting profile to the results of Rasia et al. (2004) is shown as a dotted curve.

$x \sim 0.1$, although the core temperature is hotter than that found by RTM (their best-fitting profile is shown as a dotted curve). Given AYMG also used the entropy-conserving version of GADGET (RTM did not), the difference in the slope of the inner profile could be due to the selection of objects (AYMG studied lower-mass systems),

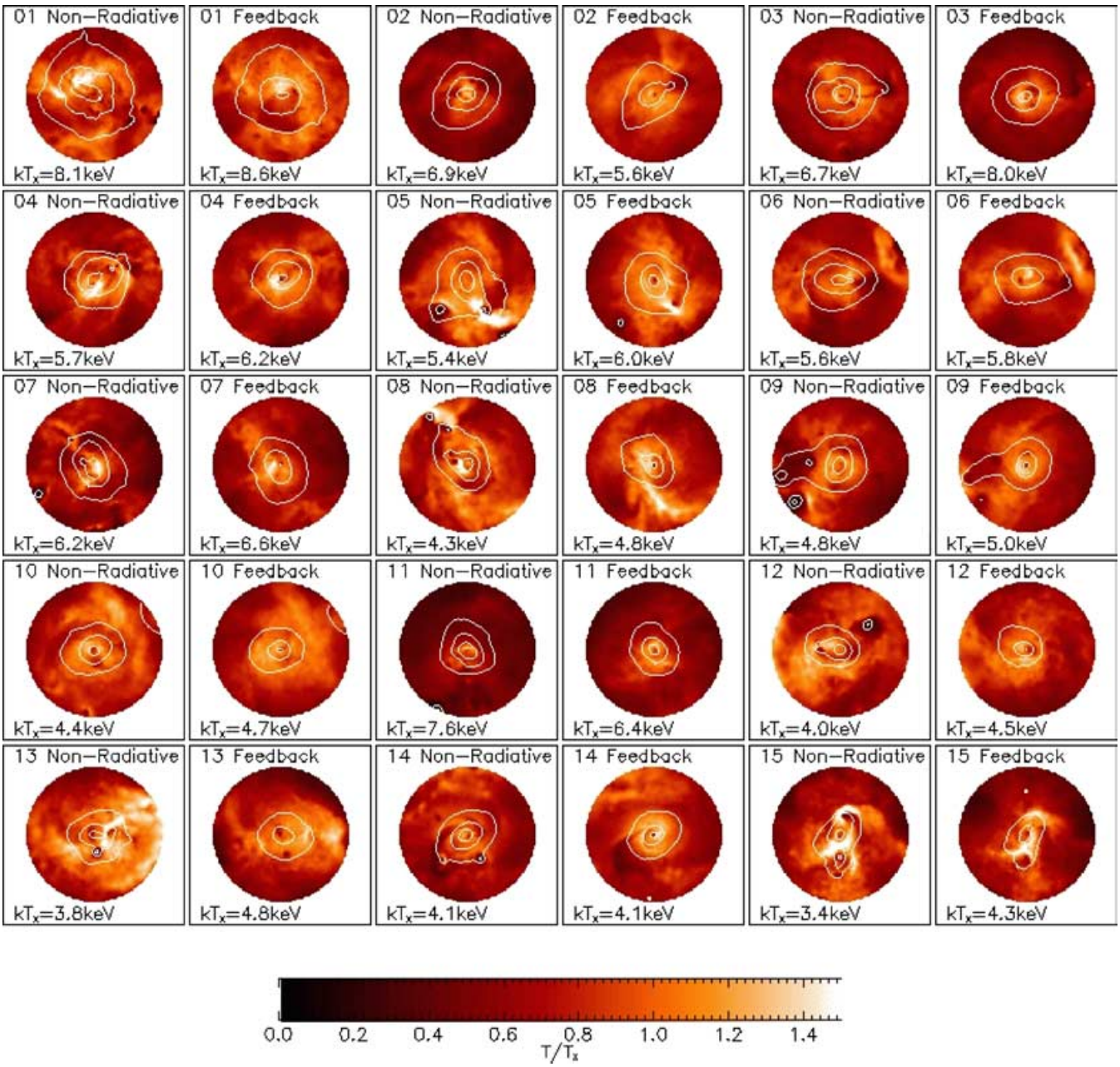

Figure 8. X-ray temperature maps for the clusters studied in this paper. Maps are shown within an Abell radius ($1.5\,h^{-1}$ Mpc). X-ray surface brightness contours (with order of magnitude intervals) are overlaid.

although we note both RTM and AYMG performed studies with both higher mass and force resolution than ours.

Including cooling and feedback produces a modest increase ($\sim$10 per cent at $x = 1$) in the temperature of the ICM. Note also that the average *feedback* profile begins to turn over within $x \sim 0.1$ due to radiative cooling.

4.2 Projected temperature profiles

To compare our temperature profiles with observations, we have constructed projected profiles. Here, we emulate the method employed by Loken et al. (2002), who themselves tried to mimic the procedure employed by Markevitch et al. (1998a). X-ray emission-weighted temperature and surface brightness maps were first constructed for the 1.5–11 keV band, using the procedure detailed by Onuora, Kay & Thomas (2003). Each map was constructed from a cube of width $4\,h^{-1}$ Mpc, centred on the cluster, and the lengths of the pixels were set to the gravitational softening, $\epsilon = 0.02\,h^{-1}$ Mpc (hence each map is 200 $\times$ 200 pixels). Maps were then centred on the pixel containing the maximum surface brightness and normalized by the X-ray emission-weighted temperature ($T_{\rm X}$) within $1\,h^{-1}$ Mpc of this centre.

The temperature maps (with surface brightness contours overlaid) are shown in Fig. 8, out to one Abell radius ($1.5\,h^{-1}$ Mpc). It is clear from this figure (see also Loken et al. 2002; Onuora et al. 2003) that the temperature of the ICM is very asymmetric and relates to the individual merger history of each cluster. How much of this information can be recovered from observed clusters, however, is a

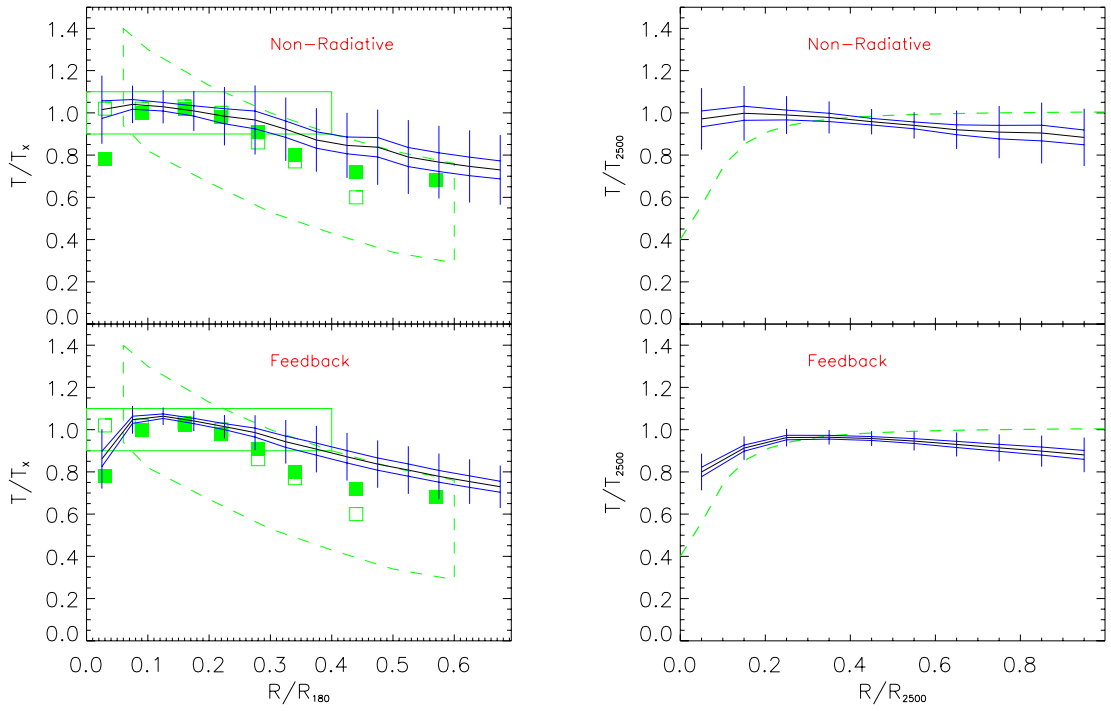

Figure 9. Projected ICM temperature profiles compared with various observational data. Left panels: profiles are plotted out to $0.7R_{180}$ and compared with results from Markevitch et al. (1998a, dashed box region), De Grandi & Molendi (2002, open and filled squares) and Arnaud et al. (2004, solid rectangle). Right panels: profiles are plotted out to R_{2500} and compared to the result from Allen et al. (2001).

question that is now only starting to be addressed (e.g. Gardini et al. 2004; Mazzotta et al. 2004).

We then constructed projected emission-weighted temperature profiles by azimuthally averaging temperatures within bins of width $0.05R_{180}$, where $R_{180} = 1.95(kT_{\rm X}/10\ {\rm keV})^{1/2}\,h^{-1}$ Mpc is the radius commonly used by observers, calibrated from the simulations of Evrard et al. (1996). The results are shown in the top panels of Fig. 9, compared to the data of Markevitch et al. (1998a), De Grandi & Molendi (2002) and Arnaud et al. (2004). Intriguingly, our mean profiles are in reasonably good agreement with the observations within $0.2R_{180}$ (excluding the cooling-flow region in the *non-radiative* model) although they fall off less rapidly in the outer parts. This is contrary to recent claims by several groups (e.g. Loken et al. 2002; AYMG; Borgani et al. 2004), who found consistency with the observations at large radii but whose profiles continued to rise into the centre. For example, Borgani et al., who included a model for both cooling and feedback in their calculation, found that the average temperature of clusters above 3 keV increased to 1.2 times the emission-weighted temperature at $\sim 0.3R_{180}$, before turning over. It is unclear whether the discrepancy is due to numerical resolution effects (Borgani et al. simulated their clusters at higher resolution) or differences in the feedback model or both. It is imperative that such discrepancies are fully understood and we aim to do so in future work.

In the bottom panels of Fig. 9, we also compare projected mass-weighted profiles to the result found by Allen et al. (2001), plotted within R_{2500}. Our *feedback* model is in reasonably good agreement at these radii (to within $\sim$10 per cent).

5 MASS ESTIMATES

We now investigate the accuracy with which our cluster masses can be recovered when making various assumptions regarding the radial

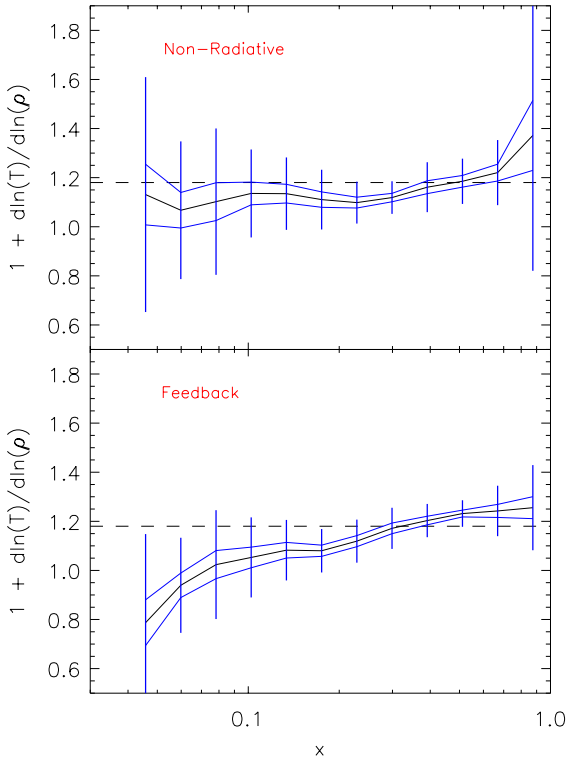

Figure 10. Effective polytropic index, γ, as a function of radius for the *non-radiative* and *feedback* models. The horizontal dashed line marks the value $\gamma = 1.18$, found to be a good description for the relaxed poor clusters studied by Ascasibar et al. (2003).

structure of the ICM. If the ICM is in hydrostatic equilibrium, the mass can be calculated from

$$M(< x) = -\frac{(x\, r_{\rm vir})^2}{G\rho(x)} \frac{{\rm d}P}{{\rm d}r}. \quad (9)$$

The simplest model would then be to assume the ICM is a polytropic gas, $P = \kappa\rho^{\gamma}$. For isothermal distributions, $\gamma = 1$, and for adiabatic distributions, $\gamma = 5/3$. We show in Fig. 10 (plotting the effective polytropic index, $\gamma = 1 + {\rm d}\ln(T)/{\rm d}\ln(\rho)$, at each radius), that this assumption is not valid in general for our simulated clusters. For the *non-radiative* systems, $\gamma \sim 1.1$ out to $x \sim 0.2$ then increases to $\gamma \sim 1.3$ at $x = 1$. For the *feedback* systems, γ increases monotonically from the centre outwards, varying from $\sim$0.8 at $x = 0.04$ to $\sim$1.3 at $x = 1$. Note that in this case γ is less than unity in the cluster core, reflecting the positive radial temperature gradient induced by cooling.

AYMG split their sample of poor clusters into relaxed, minor and major merger systems and found the first two to be well described by a single polytrope with $\gamma = 1.18$ (shown in our figure as a horizontal dashed line). For their major mergers, the main deviation in γ was in the central regions ($x \lesssim 0.3$), where the gas was close to isothermal. On average, our *non-radiative* clusters also have lower values of γ in their centres, suggesting that our objects are less relaxed than theirs, as would be expected given their higher mass and hence longer dynamical times.

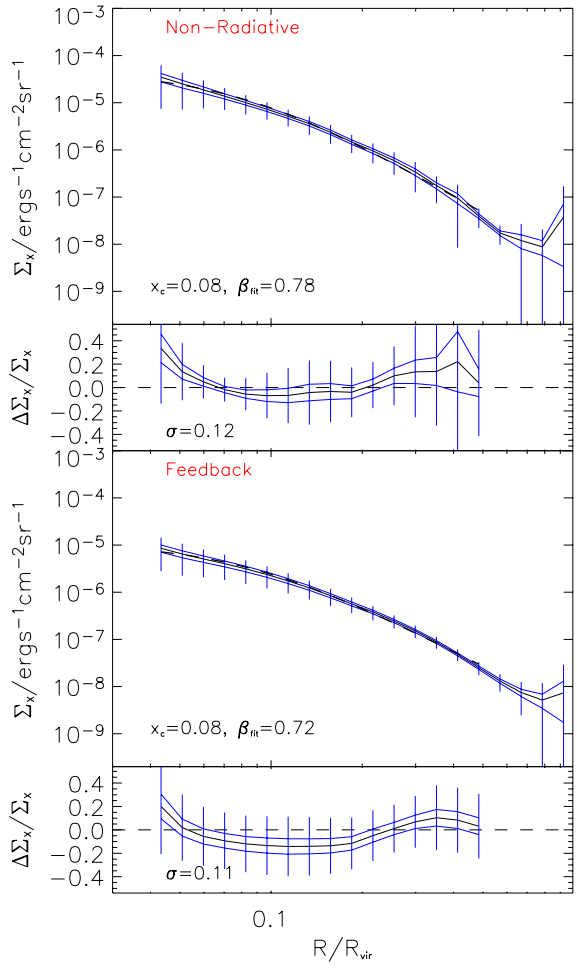

Figure 11. X-ray surface brightness profiles for clusters in the *non-radiative* and *feedback* models. Fits are only produced for $R < 0.5R_{\rm vir}$.

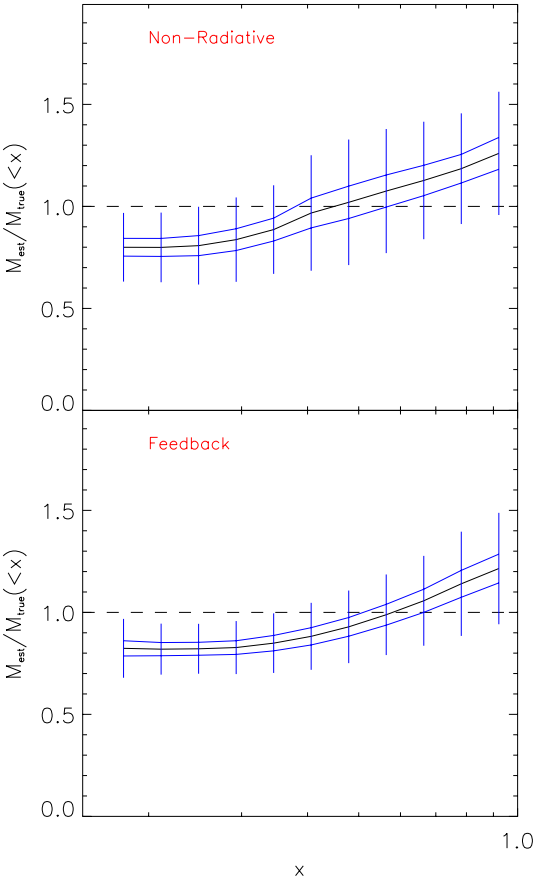

Figure 12. Ratio of estimated-to-true total cluster mass within a given radius using the isothermal β-model.

5.1 The isothermal β-model

Although our clusters are clearly not isothermal, it is nevertheless interesting to apply the isothermal β-model (Section 3.2) to equation (9) as it is this model that is most commonly used by observers to estimate cluster masses. First, the X-ray surface brightness profile is fitted:

$$\Sigma_{\rm X}(R) = \frac{\Sigma_{\rm X}(0)}{\left(R^2 + R_{\rm c}^2\right)^{3\beta_{\rm fit}-1/2}}, \quad (10)$$

where $R_{\rm c}$ is the core radius and $\beta_{\rm fit}$ is the asymptotic slope of the profile at large radii. The results from applying the same procedure to our surface brightness maps are shown in Fig. 11. As has already been shown when fitting the ICM density profile (Fig. 4), it is clear that this model does not describe the simulation data well over the whole range of radii. We only fit the data for $x < 0.5$ (at larger radii the profiles diverge due to infalling substructure); even then, the average fractional difference is around 10 per cent.

The total mass within a given radius can then be estimated:

$$M(< R) = \beta_{\rm fit} \left(\frac{3kT_{\rm X}}{G\mu m_{\rm H}}\right) \frac{R^3}{R^2 + R_{\rm c}^2}, \quad (11)$$

where $T_{\rm X}$ is a single (emission-weighted) measurement of the ICM temperature. In Fig. 12 we show results from applying equation (11) to our clusters, plotting the ratio of the estimated to the true mass within a given radius. The results are very similar for the *non-radiative* and *feedback* clusters: equation (11) underestimates the mass by $\sim$20 per cent at $x < 0.3$ and overestimates the mass by

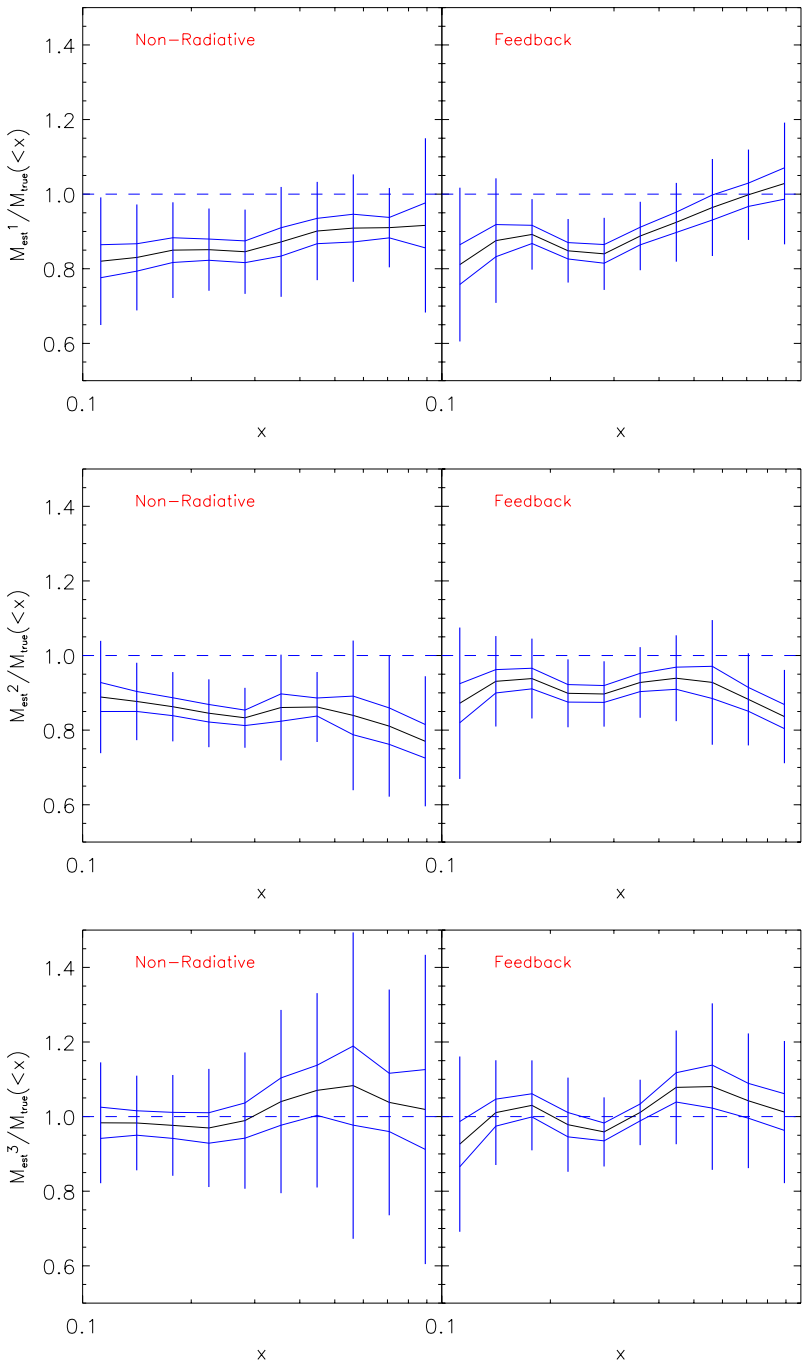

Figure 13. Ratios of estimated-to-true cluster mass as a function of radius, excluding (top panels) and including (middle panels) spatial temperature information. Results in the bottom panels are when additional, isotropic velocity dispersion information is also included.

∼30 per cent at $x = 1$. Interestingly, at $x = 0.5$ ($\sim R_{500}$) the estimated mass is within 5 per cent of the true mass. Within R_{200} ($x \sim 0.75$), masses can be estimated to better than 20 per cent. A similar study was performed by Evrard et al. (1996), who considered various models and found a similar trend with radius, albeit better agreement between the estimated and true masses at $x < 0.5$.

5.2 Single versus spatial temperature models

In the new era of *Chandra* and *XMM–Newton*, obtaining spatially resolved density and temperature information is now becoming possible. It is therefore of interest to estimate cluster masses when accurate descriptions for their density and temperature profiles are known.

Following RTM, we first perform the test where we use a single temperature to describe the ICM but use its true density profile. Equation (9) becomes

$$M_{\rm est}^{1}(<x) = \frac{kT(<x)\,x\,r_{\rm vir}}{G\mu m_{\rm H}}\,\frac{{\rm d}\ln\rho(x)}{{\rm d}\ln(x)}, \qquad (12)$$

where $T(<x)$ is the mass-weighted temperature within x. Results are shown in Fig. 13, again plotting the estimated-to-true mass ratio as a function of radius.

Our *non-radiative* result is in reasonably good agreement with the findings of RTM, with the estimated mass being lower, but within 20 per cent of the true mass for $0.1 < x < 1$. At $x < 0.3$, ratios for the *feedback* clusters are similar, but the estimated mass approaches the true mass much more rapidly at larger radius, being within ∼5 per cent between $x = 0.5$ (R_{500}) and $x = 1$. The integrated mass-weighted temperature is ∼10 per cent larger in the *feedback* clusters at all radii, increasing the estimated mass by the same factor. This is cancelled out at small radii by the flatter inner slope of the density profile. At larger radii, however, the slope increases with radius, eventually approximating the same slope as in the *non-radiative* clusters and causing the mass estimate to rise with radius.

We now include spatial temperature information in our mass estimate

$$M^2_{\rm est}(< x) = \frac{kT(x)\, x\, r_{\rm vir}}{G\mu m_{\rm H}} \left[\frac{{\rm d}\ln\rho}{{\rm d}\ln x} + \frac{{\rm d}\ln T}{{\rm d}\ln x} \right], \qquad (13)$$

with results shown in the middle panels of Fig. 13. Our *non-radiative* results are again in good agreement with RTM. Both models underpredict the mass at all radii by up to 20 per cent. Again, the mass estimate is slightly higher for the *feedback* clusters because of the increase in ICM temperature. Clearly from these results, our clusters cannot be completely in hydrostatic equilibrium. As pointed out by RTM, the isothermal mass estimator is more accurate than the non-isothermal case at larger radii, because the integrated temperature happens to cancel out the effects of gas motion.

The lack of agreement between estimated and true cluster masses is due to the presence of kinetic support, which becomes particularly significant at large radii. Radial velocity profiles confirm that our clusters are, to very good approximation, virialized systems. However, as Fig. 14 shows, the velocity dispersion of the ICM is non-negligible and becomes increasingly significant with radius. Note, however, that kinetic support is less important for the *feedback* clusters: the *non-radiative* clusters have a positive velocity dispersion gradient at all radii, whereas in the *feedback* clusters, a significant gradient appears at $x > 0.2$. Thus, the ICM in the *feedback* clusters is hydrostatic to a better approximation than in the *non-radiative* clusters.

Including an isotropic velocity dispersion term in equation (9), namely $P = \rho\,(kT/\mu m_{\rm H} + \sigma^2/3)$, we show ratios of estimated-to-true mass estimates in the bottom panels of Fig. 13. On average, the estimated masses are now in good agreement with the true masses.

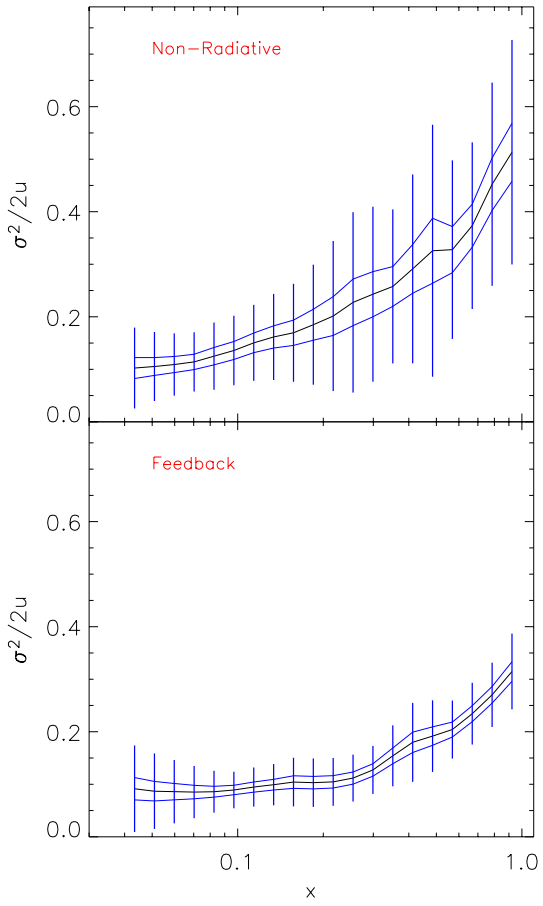

Figure 14. Ratio of kinetic-to-thermal energy, $\sigma^2/2u$, for the *non-radiative* and *feedback* clusters.

6 CONCLUSIONS

In this paper we have studied high-resolution N-body/hydrodynamical simulations of galaxy clusters to investigate the effects of radiative cooling and galactic feedback on the properties of the ICM. In particular, we compared a set of *non-radiative* simulations (the simplest model that is well-studied in the literature, but is nevertheless ruled out by X-ray observations of clusters) to our *feedback* model where a fraction (10 per cent) of cooled material is given a fixed amount of entropy (1000 keV cm^2) that is then redistributed in the ICM. The latter model reproduces the observed cluster $L_{\rm X}$–$T_{\rm X}$ relation, signifying the correct level of excess entropy in the ICM core. Our main conclusions are as follows.

(i) The distribution of total mass is, on average, reasonably well described by an NFW profile, with residual differences within 5 per cent. Including cooling and feedback does not significantly alter the shape of the cluster potential, causing only a ∼10 per cent increase in the best-fitting concentration parameter.

(ii) Cooling and feedback act to increase the entropy of the ICM everywhere, although the effect is more pronounced within the central region, where the cooling rate (and hence the rate of mass/energy injection) is higher. Outside ∼0.2 $r_{\rm vir}$, the entropy profile scales approximately linearly with radius, consistent with recent X-ray observations.

(iii) As a consequence of the excess entropy, the ICM density profile is lower and flatter in the *feedback* clusters. The isothermal β-model does not provide a good fit to the ICM density profile in either numerical models, systematically overpredicting the inner slope and underpredicting the outer slope.

(iv) Baryon fractions rise gradually from the centre outwards, reaching ∼90 per cent of the global value ($\Omega_{\rm b}/\Omega_{\rm m}$) at the virial radius. Virtually no gas is lost from the *feedback* clusters due to galactic outflows; the lower ICM gas fraction can be accounted for by the fraction of stars. However, the *feedback* model does not contain enough gas within r_{2500} to agree with the observed determinations by Allen et al. (2004), although the overall baryon fraction profiles are in good agreement. Our model overproduces the mass in stars at all radii, possibly a symptom of having such a low density threshold for star formation.

(v) Cooling and feedback produce only a modest increase in the temperature of the ICM (around 10 per cent at the virial radius) and cooling induces a positive radial temperature gradient for $r < 0.1 r_{vir}$. The temperature of the ICM is then primarily driven by gravity. Projected temperature profiles are in reasonable agreement with the observations although the decline at larger radii is not as severe.

(vi) On average, the ICM cannot be described by a single polytropic equation of state: the effective polytropic index, $\gamma = 1 + \mathrm{d}\ln(T)/\mathrm{d}\ln(\rho)$, increases with radius, reaching $\gamma \sim 1.3$ at the virial radius. Central values are lower than unity in the *feedback* clusters, due to the positive radial temperature gradient induced by radiative cooling.

(vii) Estimating the total mass of clusters by fitting surface brightness profiles with the isothermal β-model is accurate to within 20–30 per cent (depending on the outer radius chosen), regardless of the simulated model. The model is most accurate around $r = 0.5r_{\rm vir}$ ($\sim r_{500}$), where the error is $\sim$5 per cent.

(viii) As found by Rasia et al. (2004), the ICM is not completely hydrostatic, leading to an underestimate in the true mass of the cluster of up to 20 per cent in our *non-radiative* clusters, even when full density and temperature information is included in the calculation. Including a kinetic pressure term recovers the true mass. The degree of thermalization in the ICM improves when cooling and feedback are included, predicting a hydrostatic mass that is within 10 per cent of the true mass for $r < r_{500}$.

In summary, we find that cooling and feedback mainly affect the inner structure of the ICM, as a consequence of the excess entropy produced by these processes. Although our *feedback* model approximately achieves the overall desired entropy excess in clusters, it does not provide a detailed match to the inner structure of the ICM, namely the gas mass fraction within r_{2500} is around 60 per cent of the observed value (Allen et al. 2004). Whether this discrepancy can be rectified within the context of our feedback model (by varying the model parameters and/or increasing the numerical resolution of the simulations), or whether our simulations are still missing some fundamental physical process, requires further investigation.

ACKNOWLEDGMENTS

We thank the referee, Stefano Borgani, for his insightful comments that improved the quality of the manuscript. We also thank Volker Springel for generously allowing us to use GADGET2 before its public release and for his help with various technical issues, and Steve Allen for providing observational data. Simulation data were generated using COSMA, the 670-processor COSmology MAchine at the Institute for Computational Cosmology in Durham. The work presented in this paper was carried out as part of the programme of the Virgo Supercomputing Consortium (http://www.virgo.dur.ac.uk). STK and ARJ are supported by PPARC, FRP is a PPARC Advanced Fellow.

REFERENCES

Allen S. W., Schmidt R. W., Fabian A. C., 2001, MNRAS, 328, L37
Allen S. W., Schmidt R. W., Fabian A. C., 2002, MNRAS, 334, L11
Allen S. W., Schmidt R. W., Fabian A. C., Ebeling H., 2003, MNRAS, 342, 287
Allen S. W., Schmidt R. W., Ebeling H., Fabian A. C., van Speybroeck L., 2004, MNRAS, 353, 457
Arnaud M., Evrard A. E., 1999, MNRAS, 305, 631
Arnaud M., Pratt G. W., Pointecouteau E., 2004, Mem. Soc. Astron. Ital., 75, 529
Ascasibar Y., Yepes G., Müller V., Gottlöber S., 2003, MNRAS, 346, 731 (AYMG)
Balogh M. L., Pearce F. R., Bower R. G., Kay S. T., 2001, MNRAS, 326, 1228
Benson A. J., Bower R. G., Frenk C. S., Lacey C. G., Baugh C. M., Cole S., 2003, ApJ, 599, 38
Bialek J. J., Evrard A. E., Mohr J. J., 2001, ApJ, 555, 597
Binney J., 1977, ApJ, 215, 483
Binney J., 2004, MNRAS, 347, 1093
Borgani S., Governato F., Wadsley J., Menci N., Tozzi P., Lake G., Quinn T., Stadel J., 2001, ApJ, 559, L71
Borgani S., Governato F., Wadsley J., Menci N., Tozzi P., Quinn T., Stadel J., Lake G., 2002, MNRAS, 336, 409
Borgani S. et al., 2004, MNRAS, 348, 1078
Bower R. G., 1997, MNRAS, 288, 355
Bower R. G., Benson A. J., Lacey C. G., Baugh C. M., Cole S., Frenk C. S., 2001, MNRAS, 325, 497
Bryan G. L., Norman M. L., 1998, ApJ, 495, 80
Bryan G. L., 2000, ApJ, 544, L1
Cavaliere A., Fusco–Femiano R., 1976, A&A, 49, 137
Cen R., Ostriker J. P., 1994, ApJ, 429, 4
Cole S. M., 1991, ApJ, 367, 45
Davé R., Katz N., Weinberg D. H., 2002, ApJ, 579, 23
De Grandi S., Molendi S., 2002, ApJ, 567, 163
Edge A. C., Stewart G. C., 1991, MNRAS, 252, 414
Eke V. R., Cole S., Frenk C. S., 1996, MNRAS, 282, 263
Eke V. R., Navarro J. F., Frenk C. S., 1998, ApJ, 503, 569
Ettori S., 2003, MNRAS, 344, L13
Evrard A. E., 1989, ApJ, 341, L71
Evrard A. E., 1990, ApJ, 363, 349
Evrard A. E., Henry J. P., 1991, ApJ, 383, 95
Evrard A. E., Metzler C. A., Navarro J. F., 1996, ApJ, 469, 494
Evrard A. E., 1997, MNRAS, 292, 289
Fabian A. C., 2003, in Avila-Reese, V., Firmani, C., Frenk, C. S., Allen, C., eds, Galaxy Evolution: Theory and Observations, Revista Mexicana de Astronomía y Astrofísica (Serie de Conferencias) Vol. 17, p. 303
Fardal M. A., Katz N., Gardner J. P., Hernquist L., Weinberg D. H., Davé R., 2001, ApJ, 562, 605
Frenk C. S. et al., 1999, ApJ, 525, 554
Gao L., De Lucia G., White S. D. M., Jenkins A., 2004, MNRAS, 352, L1
Gardini A., Rasia E., Mazzotta P., Tormen G., de Grandi S., Moscardini L., 2004, MNRAS, 351, 505
Henry J. P., Arnaud K. A., 1991, ApJ, 372, 410
Henry J. P., 2000, ApJ, 534, 565
Henry J. P., 2004, ApJ, 609, 603
Irwin J. A., Bregman J. N., Evrard A. E., 1999, ApJ, 519, 518
Irwin J. A., Bregman J. N., 2000, ApJ, 538, 543
Jenkins A., Frenk C. S., White S. D. M., Colberg J. M., Cole S., Evrard A. E., Couchman H. M. P., Yoshida N., 2001, MNRAS, 321, 372
Kaiser N., 1986, MNRAS, 222, 323
Kaiser N., 1991, ApJ, 383, 104
Katz N., White S. D. M., 1992, ApJ, 412, 455
Kay S. T., Pearce F. R., Jenkins A., Frenk C. S., White S. D. M., Thomas P. A., Couchman H. M. P., 2000, MNRAS, 316, 374
Kay S. T., Thomas P. A., Theuns T., 2003, MNRAS, 343, 608
Kay S. T., 2004, MNRAS, 347, L13
Lewis G. F., Babul A., Katz N., Quinn T., Hernquist L., Weinberg D. H., 2000, ApJ, 536, 623
Lin Y. T., Mohr J. J., Stanford S. A., 2003, ApJ, 591, 749
Loken C., Norman M. L., Nelson E., Burns J., Bryan G. L., Motl P., 2002, ApJ, 579, 571
Markevitch M., Forman W. R., Sarazin C. L., Vikhlinin A., 1998a, ApJ, 503, 77
Markevitch M., 1998b, ApJ, 504, 27
Mazzotta P., Rasia E., Moscardini L., Tormen G., 2004, MNRAS, 354, 10
Muanwong O., Thomas P. A., Kay S. T., Pearce F. R., Couchman H. M. P., 2001, ApJ, 552, L27
Muanwong O., Thomas P. A., Kay S. T., Pearce F. R., 2002, MNRAS, 336, 527
Murante G. et al., 2004, ApJ, 607, L83
Navarro J. F., Frenk C. S., White S. D. M., 1995, MNRAS, 275, 720
Navarro J. F., Frenk C. S., White S. D. M., 1997, ApJ, 490, 493 (NFW)
Onuora L. I., Kay S. T., Thomas P. A., 2003, MNRAS, 341, 1246
Oukbir J., Blanchard A., 1992, A&A, 262, L21

Pearce F. R., Thomas P. A., Couchman H. M. P., Edge A. C., 2000, MNRAS, 317, 1029
Pierpaoli E., Borgani S., Scott D., White M., 2003, MNRAS, 342, 163
Ponman T. J., Cannon D. B., Navarro J. F., 1999, Nat, 397, 135
Ponman T. J., Sanderson A. J. R., Finoguenov A., 2003, MNRAS, 343, 331
Press W. H., Schechter P., 1974, ApJ, 187, 425
Rasia E., Tormen G., Moscardini L., 2004, MNRAS, 351, 237 (RTM)
Sheth R. K., Mo H. J., Tormen G., 2001, MNRAS, 323, 1
Spergel D. N. et al., 2003, ApJS, 148, 175
Springel V., Yoshida N., White S. D. M., 2001, New Astron., 6, 79
Springel V., Hernquist L., 2002, MNRAS, 333, 649
Springel V., Hernquist L., 2003, MNRAS, 333, 289
Suginohara T., Ostriker J. P., 1998, ApJ, 507, 16
Sutherland R. S., Dopita M. A., 1993, ApJS, 88, 253
Thomas P. A., Couchman H. M. P., 1992, MNRAS, 257, 11
Thomas P. A., Muanwong O., Pearce F. R., Couchman H. M. P., Edge A.C., Jenkins A., Onuora L., 2001, MNRAS, 324, 450
Thomas P. A., Muanwong O., Kay S. T., Liddle A. R., 2002, MNRAS, 330, L48
Tornatore L., Borgani S., Springel V., Matteucci F., Menci N., Murante G., 2003, MNRAS, 342, 1025
Tozzi P., Norman C., 2001, ApJ, 546, 63
Verde L., 2003, New Astron. Rev., 47, 713
Viana P. T. P., Liddle A. R., 1996, MNRAS, 281, 323
Viana P. T. P., Kay S. T., Liddle A. R., Muanwong O., Thomas P. A., 2003, 346, 319
Voit G. M., Bryan G. L., 2001, Nat, 6862, 425
Voit G. M., Bryan G. L., Balogh M. L., Bower R. G., 2002, ApJ, 576, 601
Voit G. M., Balogh M. L., Bower R. G., Lacey C. G., Bryan G. L., 2003a, ApJ, 593, 272
Voit G. M., Ponman T. J., 2003b, ApJ, 594, L75
Voit G. M., Kay S. T., Bryan G. L., 2004, ApJ, submitted
White D. A., 2000, MNRAS, 312, 663
White S. D. M., Frenk C. S., 1991, ApJ, 379, 52
White S. D. M., Efstathiou G., Frenk C. S., 1993a, MNRAS, 262, 1023
White S. D. M., Navarro J. F., Evrard A. E., Frenk C. S., 1993b, Nat, 366, 429
Wu K. K. S., Fabian A. C., Nulsen P. E. J., 2000, MNRAS, 318, 889
Wu X.-P., Xue Y.-J., 2002, ApJ, 569, 112
Yoshida N., Sheth R. K., Diaferio A., 2001, MNRAS, 328, 669

This paper has been typeset from a TEX/LATEX file prepared by the author.